

## Article

# Advanced Method of Variable Refrigerant Flow (VRF) Systems Designing to Forecast Onsite Operation—Part 2: Phenomenological Simulation to Recoup Refrigeration Energy

Mykola Radchenko <sup>1</sup>, Andrii Radchenko <sup>1</sup>, Eugeny Trushliakov <sup>2</sup>, Hanna Koshlak <sup>3,\*</sup> and Roman Radchenko <sup>1</sup>

<sup>1</sup> Machinebuilding Institute, Admiral Makarov National University of Shipbuilding, Heroes of Ukraine Avenue 9, 54025 Mykolayiv, Ukraine

<sup>2</sup> Department of Air Conditioning and Refrigeration, Admiral Makarov National University of Shipbuilding, Heroes of Ukraine Avenue 9, 54025 Mykolayiv, Ukraine

<sup>3</sup> Department of Sanitary Engineering, Kielce University of Technology, Al. Tysiąclecia Państwa Polskiego 7, 25-314 Kielce, Poland

\* Correspondence: hkoshlak@tu.kielce.pl

**Abstract:** This paper focuses on the application of speed-regulated compressors (SRCs) to cover changeable heat loads with high efficiency in conventional air conditioning systems (ACS) as well as in the more advanced variable refrigerant flow (VRF)-type outdoor and indoor ACS. In reality, an SRC is an oversized compressor, although it can operate efficiently at part loads. The higher the level of regulated loads (LRL) of the SRC, the more the compressor is oversized. It is preferable to reduce the size of the SRC by covering the peak loads and recouping the excessive refrigeration energy reserved at decreased actual loads within the range of regulated loads. Therefore, the range of changeable loads is chosen as the object to be narrowed by using the reserved refrigeration capacity. Thus, the general fundamental approach of dividing the overall heat load range of the ACS into the ranges with changeable and unchangeable loads, as previously developed by the authors, is applied for the range of primary changeable loads. Due to this innovative step, the principle of two-stage outdoor air conditioning according to changeable and unchangeable loads, also proposed by the authors, has been extended over the range of primary changeable loads to reduce the level of refrigeration capacity regulation and SRC size. To realize this, part of the changeable load range is offset by the reserved refrigeration capacity, leading to a reduction in the changeable load range and the SRC size by approximately 20% for temperate climatic conditions.

**Keywords:** air conditioning system; load range; refrigeration capacity excess; threshold temperature; level of loading



**Citation:** Radchenko, M.; Radchenko, A.; Trushliakov, E.; Koshlak, H.; Radchenko, R. Advanced Method of Variable Refrigerant Flow (VRF) Systems Designing to Forecast Onsite Operation—Part 2: Phenomenological Simulation to Recoup Refrigeration Energy. *Energies* **2023**, *16*, 1922. <https://doi.org/10.3390/en16041922>

Academic Editors: Chi-Ming Lai and Christopher Micallef

Received: 26 December 2022

Revised: 31 January 2023

Accepted: 11 February 2023

Published: 15 February 2023



**Copyright:** © 2023 by the authors. Licensee MDPI, Basel, Switzerland. This article is an open access article distributed under the terms and conditions of the Creative Commons Attribution (CC BY) license (<https://creativecommons.org/licenses/by/4.0/>).

## 1. Introduction

Air conditioning systems (ACSs) are the most widespread systems applied in buildings to maintain comfort parameters [1,2] and in engine rooms to support low-intake air temperatures, enabling the efficient operation of engines [3,4]. Their widespread application in the conditioning of cyclic air in combustion engines, particularly in internal combustion engines [5,6] and gas turbines [7,8], has led to the requirement for the development of ACSs as subsystems of trigeneration plants [9,10] for the combined cooling, heating, and power (CCHP) supply of districts [11,12]. Such a wide use of ACSs in energetic applications, including stationary [13,14] and transport power plants [15,16], is a result of the significant exhaust heat potential available for conversion to refrigeration by chillers [17,18] due to the application of highly efficient economizers and low-temperature heating surfaces [19,20]. This excessive refrigeration led to the widening of its application in traditional building and engine-sucked air conditioning [21,22].

The changeable loads on the ACS and heat exchangers accordingly lead to falling heat fluxes and require the application of highly efficient heat exchangers and working

fluid circulation circuits. The application of advanced heat exchangers [23,24], initially by compact evaporators [25,26] and minichannel-type condensers [27,28], led to an increased interest in research focused on intensifying heat transfer [29,30] and hydrodynamics [31,32] under conditions of unstable two-phase flows [33,34], uneven refrigerant [35,36], and airflow distribution [37,38]. A considerable number of innovative air conditioning and refrigerant supply [39,40] circuits have been proposed, particularly with the application of ejectors [41,42] and thermopressors [43,44] as circulation devices using the potential energy of high-pressure fluids [45,46].

The performance of energy conversion systems [47,48], including ACSs, is characterized by off-design modes [49,50] especially evident in mild and off-season climatic conditions.

Various thermal demand and primary energy-saving (TDM and PES) management methods [51,52], criteria [53,54], and indicators [55,56] were proposed for providing a high level of loading [57,58] and estimating the effect gained due to the application of combined energy systems [59,60] performance efficiency, including ACSs as subsystems [61,62] or autonomic variable refrigerant flow (VRF)-type ACSs with SRCs [63,64].

The VRF systems are considered the most efficient for off-season operation [65,66]. Their combined version includes two subsystems for outdoor and indoor air processing [67,68]. The outdoor system treats the outdoor air and offsets fluctuated heat loads in order to avoid overloading the indoor system [69,70]. The VRF system provides an energy saving of more than 20% compared to the variable air volume ACS [71–74].

The method used to estimate the performance efficiency of SRCs through imposing the load ranges, regulated by the SRC, on the ranges of changeable and unchangeable loads within the overall range of actual loading was previously developed by the authors. With this, the efficiency of SRC operation is estimated by the rate of loading the unregulated range assumed as the object of investigation [75].

In reality, the SRC is an oversized compressor, although it operates efficiently at part loads. The higher the level of regulated loads (LRL) of the SRC, the more oversized the compressor. It is preferable to reduce its size through the application of the SRC with LRL = 0.5 instead of LRL = 0.7. This might be possible by reducing the range of fluctuating loads and increasing its level of loading (LL). The latter is possible by covering the peak loads using the exceeding refrigeration energy reserved at lowered actual loads. Thus, the enhancement of the operation efficiency of the advanced VRF system with a modern SRC and reduced size may be achieved by recouping the refrigeration energy excess.

The aim of the research is to enhance the operation efficiency of VRF systems with SRCs by recouping the refrigeration energy reserved at lowered loading to reduce the range of outdoor air preconditioning at changeable heat loads and the level of regulated load (LRL) and SRC sizes as a result.

## 2. Methods

The following approaches and assumptions have been accepted in the design methodology of advanced ACSs to simplify quantifying the analysis results.

In order to obtain a direct and a simple tool and a more precise method for minimizing the errors caused by the approximation of the actual primary data, the fluctuations of data on actual refrigeration energy consumption  $Q_0 \cdot \tau$  is considered by the rate of the summarized annual values versus the refrigeration capacity  $Q_0$ :

$$\Sigma(Q_0 \cdot \tau) = f(Q_0). \quad (1)$$

Such an approach enables the treatment of the annual refrigeration energy cumulative characteristic (1) independent of the rate of annual refrigeration energy increment and allows the determination of the optimal value of refrigeration capacity  $Q_{0,opt}$ , associated with the maximum rate of cumulative curve  $\Sigma(Q_0 \cdot \tau) = f(Q_0)$ , and a precise value of rational refrigeration capacity  $Q_{0,rat}$ , avoiding its overestimation accompanied by a negligible increment of annual output.

Thus, the annual refrigeration energy consumption  $\Sigma(Q_0 \cdot \tau)$  is considered a primary criterion to design the refrigeration capacity of an ACS.

The next stage of ACS designing focuses on the rational distribution of the overall design refrigeration capacity according to the peculiarities of heat loading in response to current climatic conditions. The distribution of the total design refrigeration capacity between the range of changeable loads, affected by outdoor air parameter variations and covered by the speed-regulated compressor (SRC) and the range of unchangeable loads of further subconditioned air to the set temperature, is the result of the second stage of ACS designing.

The method for shearing the overall range of actual thermal loads on the ACS into the ranges of changeable loads for ambient air precooling and the unchangeable load for further air subcooling to the target temperature  $t_{a2}$ , accordingly, was developed for adopting the designed refrigeration capacity to cover both of them [75].

The value of the threshold temperature  $t_{thr}$  to share the overall range of the designed thermal load  $q_{0.10rat}$  into the ranges with different characters of loading is first determined by stabilizing the loads below its magnitude. Thus, the threshold temperature  $t_{thr}$  is used as an indicator for sharing the overall load range of outdoor air conditioning into the ranges with different characters of loading.

The method for the distribution of the overall design heat load (design refrigeration capacity) developed by the authors [75] is expanded to narrow the range of changeable loads through recouping the excessive refrigeration energy obtained at lower current loads to cover peak loads within the additional range of an artificially stabilized heat load. As a result, the residual part of the range with initially changeable loads becomes considerably narrower than the primary load, leading to a reduction in the ratio of the changeable load range, covered by the RSC, to the overall load range, id est, the required level of regulated loads (LRL).

Based on the fact that any heat loading influenced by current climatic conditions has changeable behavior, inevitably accompanied by the formation of refrigeration energy excesses, the next step of the analysis is focused on realizing these reserves through the recoup of the increased heat loads.

Thus, the concept of two-stage outdoor air conditioning [75] has received renewed interest in terms of broadening its application within the primary range of changeable loads; it can be narrowed using the excessive refrigeration energy obtained at lowered current loads to cover the peak loads. This leads to a reduction in the ratio of the changeable load range, covered by the RSC, to the overall load range including the unchangeable loads.

The specific refrigeration capacity  $q_0$  as the total value of the refrigeration capacity  $Q_0$ , referred to as unit air mass flow rate ( $G_a = 1 \text{ kg/s}$ ), i.e.,  $q_0 = Q_0/G_a$ , is used in the following calculations:

$$q_0 = \xi \cdot c_a \cdot (t_a - t_{a2}), \text{ kW}/(\text{kg/s}), \quad (2)$$

where  $t_a$ —initial or ambient  $t_{amb}$  air temperature, K or °C;  $t_{a2}$ —a set air temperature, accepted as an example in the investigation equal to  $t_{a2} = 10 \text{ °C}$ ;  $\xi$ —relative heat ratio as the total heat, removed from the air, related to its sensible heat; and  $c_a$ —air-specific heat,  $\text{kJ}/(\text{kg} \cdot \text{K})$ .

Specific annual and monthly refrigeration energy consumption is calculated as:

$$\Sigma(q_0 \cdot \tau) = \Sigma \xi c_a \cdot (t_a - t_{a2}) \cdot \tau \cdot 10^{-3}, \text{ kWh}/(\text{kg/s}).$$

Accordingly, the specific values of refrigeration capacity  $q_{0.10}$  and refrigeration energy consumption  $q_{0.10} \cdot \tau$  are needed for cooling air to  $t_{a2} = 10 \text{ °C}$ .

This enables the generalization of the results and their widespread application for any value of air mass flow rate  $G_a$  and total refrigeration capacity  $Q_0 = q_0 G_a$  as a result.

According to the proposed method, the changes in the actual specific refrigeration energy consumption  $q_0 \cdot \tau$  are taken into account by the rate of their annual summation  $\Sigma(q_0 \cdot \tau)$  increment. With this, a cumulative energetic characteristic of the ACS as a dependence of

specific annual refrigeration energy consumption  $\Sigma(q_0 \cdot \tau)$  on the design (installed) specific refrigeration capacity  $q_0$  is used as a basic factor to determine a rational  $q_{0,\text{rat}}$  design value:  $\Sigma(q_0 \cdot \tau) = f(q_0)$  (Figure 1) [75].

The values of rational  $q_{0,\text{rat}}$  specific refrigeration capacities when conditioning outdoor air were calculated for temperate climatic conditions in southern Ukraine (the Mykolayiv region) in 2017 (Figure 1).

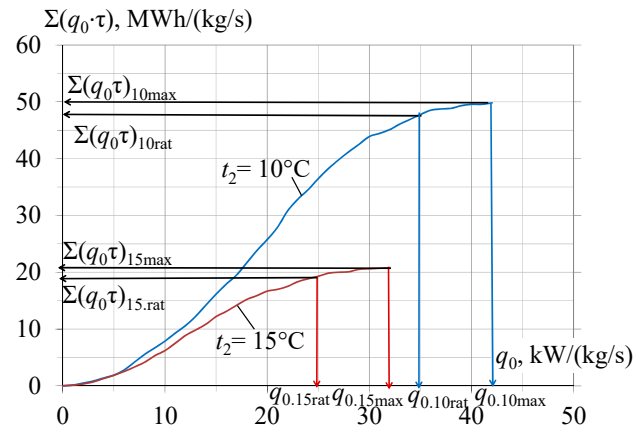


**Figure 1.** Specific annual refrigeration energy consumption  $\Sigma(q_0 \cdot \tau)$  and the rational values  $q_{0,\text{rat}}$  when conditioning air to  $t_{a2} = 10, 15^\circ\text{C}$ , and  $20^\circ\text{C}$ .

The rational value  $q_{0,\text{rat}}$  of the design refrigeration capacity is able to offset the annual refrigeration consumption  $\Sigma(q_0 \tau)_{\text{rat}} = 48 \text{ MWh}/(\text{kg}/\text{s})$  close to its maximum value of  $50 \text{ MWh}/(\text{kg}/\text{s})$ , but at a reduced design refrigeration capacity  $q_{0,10\text{rat}} = 35 \text{ kW}/(\text{kg}/\text{s})$  less than  $q_{0,10\text{max}} = 42 \text{ kW}/(\text{kg}/\text{s})$  (Figure 1).

Further development of the methodology for the rational design of an ACS that regulates the refrigeration capacity aims to develop the method for shearing the total design refrigeration capacity according to current heat loads into ranges with different change behaviors. The range of fluctuations of the heat load requires the application of a speed-regulated compressor (SRC). The range of a relatively stable heat load for deeper air cooling to the final temperature, for example  $t_{a2} = 10^\circ\text{C}$ , can be covered by a conventional compressor without refrigeration capacity regulation.

In order to apply the compressor with refrigeration capacity regulation to offset both loading ranges, it is necessary to analyze the ratio between both ranges and compare it to the level of refrigeration capacity regulation by the SRC, i.e., the load regulation level (LRL).

The SRC with  $\text{LRL} = 0.5$  is assumed to simplify the analyses at the initial step of approximation. Accordingly, the changeable load range, from  $\text{LRL} \cdot q_{0,10\text{rat}} = 0.5 q_{0,10\text{rat}}$  up to  $q_{0,10\text{rat}}$ , is considered the level of regulated load covered by the SRC, whereas a range of load below (outside) the SRC-regulated range, from  $1 - \text{LRL} \cdot q_{0,10\text{rat}} = 0.5 q_{0,10\text{rat}}$  or  $q_{0,10\text{rat}}/2 = 0.5 q_{0,10\text{rat}}$  down to  $q_0 = 0$ , designed as the stable range, must be analyzed by the level of loading for the estimation of the SRC's operation efficiency.

It should be noted that fluctuations (drops) of heat load in the range  $q_{0,10-15} = q_{0,10} - q_{0,15}$  of further deeper air conditioning below the threshold temperature  $t_{\text{thr}} = 15^\circ\text{C}$  indicate the excess of the designed refrigeration capacity  $q_{0,15\text{rat}}$  over its current values  $q_{0,15}$ . The latter is revealed at the booster stage of preconditioning the outdoor air to  $t_{\text{thr}} = 15^\circ\text{C}$ , calculated on the residual principle as  $q_{0,b10-15\text{rat}} = q_{0,10} - q_{0,10-15}$  (Figure 2).

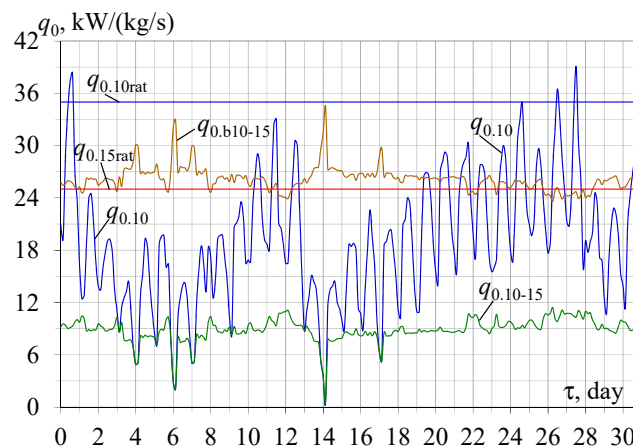


**Figure 2.** Current values of specific refrigeration capacities  $q_{0,10}$  required for outdoor air conditioning to 10 °C, refrigeration capacities  $q_{0,10-15}$  for subsequent air conditioning from 15 °C to 10 °C, and available booster values  $q_{0,b10-15}$  remained for outdoor air conditioning to 15 °C:  $q_{0,10-15} = q_{0,10} - q_{0,15}$ ;  $q_{0,b10-15} = q_{0,10} - q_{0,10-15}$ .

### 3. Results and Discussion

The total values of the specific refrigeration capacities  $q_{0,10}$ , needed for conditioning outdoor air to 10 °C, can be sheared into the range of changeable values  $q_{0,15}$ , needed for preconditioning outdoor air to 15 °C, and practically unchangeable refrigeration capacities  $q_{0,10-15}$  for the subsequent conditioning of air from 15 °C to 10 °C. The calculation results for July 2017 in climatic conditions in the Mykolayiv region, southern Ukraine, as example of a temperate climate, are presented in Figure 2.

As Figure 2 shows, the current total fluctuated heat load  $q_{0,10}$  for conditioning outdoor air to 10 °C can be shared in the range of the fluctuated load for preconditioning outdoor air to 15 °C, and the range of practically unchangeable heat load  $q_{0,10-15}$  for subsequent air conditioning from 15 °C to 10 °C. Accordingly, the latter is to be accepted as the basic, practically unchangeable part,  $q_{0,10-15} \approx q_{0,10rat} - q_{0,15rat}$ , of the total rational design value  $q_{0,10rat}$ , whereas the rest, as remainder of the rational design value  $q_{0,10rat}$ , might be used as the residual booster  $q_{0,b10-15} = q_{0,10rat} - q_{0,10-15}$  available for preconditioning outdoor air to 15 °C.

Basing on the above, the intermediate temperature of 15 °C might be accepted as the threshold  $t_{thr}$ , stabilizing the heat loads in the further conditioning of outdoor air below  $t_{thr} = 15$  °C, and as an indicator to share the overall range of the design heat load  $q_{0,10rat}$  (Figure 1) in two ranges according to the different loading characteristics.

In terms of the changeable loading characteristics, accompanied by the inevitable excesses of the designed refrigeration capacity  $q_{0,10rat}$  over the actual loads  $q_{0,10}$ , reflected in the booster refrigeration capacity  $q_{0,b10-15} = q_{0,10rat} - q_{0,10-15}$  available for preconditioning outdoor air to 15 °C, the latter is accepted as the object for analysis to use the excess refrigeration capacity for covering the peak loads.

The range of load, regulated by the SRC, is characterized by the level of regulated load as a ratio of the load regulated to the overall load  $q_{0,10}$ , including the unregulated load.

The operation efficiency of the SRC with a definite design LRL (LRL = 0.5, for example) is at its maximum when the loads  $q_{0,10} < 0.5$  are within a range from  $q_0 = 0$  to  $q_{0,10rat}/2$ , equal to  $q_{0,10rat}/2$  (Figure 3).

The consumption of refrigeration capacity  $q_{0,10} < 0.5$  within a range without its regulation (from 0 to  $q_{0,10rat}/2$ ) is marked as  $q_{0,10} < 0.5$ .

A lack of loads within its unregulated range  $q_{0,10} < q_{0,10rat}/2$  is considered to exceed  $q_{0,10rat}/2_{ex} < 0.5 = q_{0,10rat}/2 - q_{0,10} < 0.5$  of the rational design value of the refrigeration capacity  $q_{0,10rat}/2$  over the actual loads  $q_{0,10} < 0.5$  (Figure 3).

The monthly summarized values of the designed refrigeration energy generation exceedance  $\sum(q_{0,10rat}/2\tau)_{ex} < 0.5$  of the refrigeration energy  $\sum(q_{0,10rat}/2\tau)$ , generated according

to the design value  $q_{0.10rat}/2$  above the consumed values  $\sum(q_{0.10<0.5}\tau)$ , reflect the trend in the ratio of reserved and consumed refrigeration energy under onsite climatic conditions.

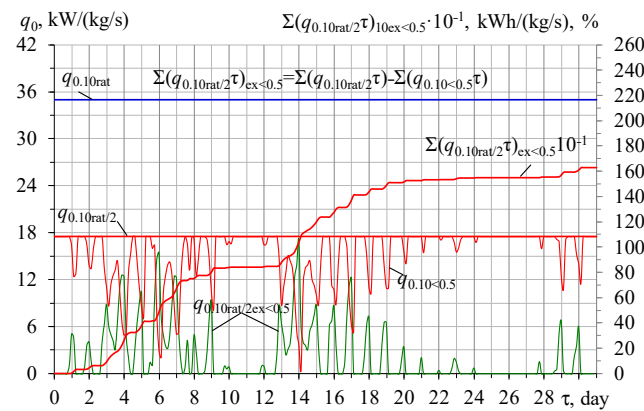


**Figure 3.** Actual values of refrigeration capacity consumption  $q_{0.10<0.5}$  and exceedance of rational refrigeration capacity  $q_{0.10rat}/2_{ex<0.5}$  within a range without regulation ( $q_{0.10} < q_{0.10rat}/2$ ), monthly summarized values of exceedance  $\sum(q_{0.10rat}/2\tau)_{ex<0.5}$ :  $q_{0.10rat}/2_{ex<0.5} = q_{0.10rat}/2 - q_{0.10<0.5}$ ;  $\sum(q_{0.10rat}/2\tau)_{ex<0.5} = \sum(q_{0.10rat}/2\tau - q_{0.10<0.5}\tau)_{ex<0.5}$ ;  $q_{0.10rat}/2 = 0.5q_{0.10rat}$ ;  $q_{0.10<0.5}$ —marked for  $q_{0.10} < 0.5q_{0.10rat}$ .

The continuously growing character of the curve of the monthly summarized refrigeration energy exceedance  $\sum(q_{0.10rat}/2\tau)_{ex<0.5}$  (Figure 3) exposes the refrigeration reserve for partly covering the daily fluctuated heat loads when preconditioning outdoor air to 15 °C. This leads to a narrowing of the range of the changeable load and the value of the LRL.

The relative values of the summarized consumed refrigeration energy  $\sum(q_{0.10<0.5}\tau)_{<0.5} / \sum(q_{0.10rat}/2\tau)$  characterize the level of loading in the range of the unregulated load,  $LL = \sum(q_{0.10<0.5}\tau)_{<0.5} / \sum(q_{0.10rat}/2\tau)$  (Figure 4).

Accordingly, the lack of heat loading in the range of the unregulated load, considered as the exceedance  $q_{0.10rat}/2_{ex<0.5}$  of the design load (refrigeration capacity)  $q_{0.10rat}$  above the actual heat loads (refrigeration consumption)  $q_{0.10<0.5}$ , can be characterized by the relative values of the summarized excess of the refrigeration energy  $\sum(q_{0.10rat}/2\tau)_{ex<0.5} / \sum(q_{0.10rat}/2\tau)$  generated according to the design value  $q_{0.10rat}/2$ . In reality, these relative values characterize the reduction of the load level  $LL_{red} = \sum(q_{0.10rat}/2\tau)_{ex<0.5} / \sum(q_{0.10rat}/2\tau)$  and, accordingly, can be calculated by the correlation  $LL_{red} = 1 - LL$  (Figure 4). This will be used in further analyses.

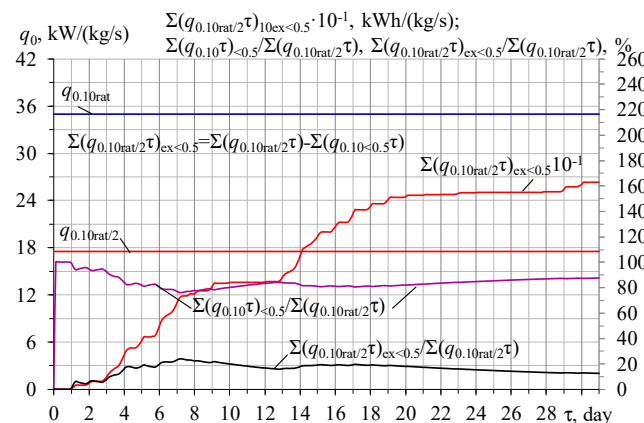


**Figure 4.** Monthly summarized values of design refrigeration energy exceedance  $\sum(q_{0.10rat}/2\tau)_{ex<0.5}$  above consumed values  $\sum(q_{0.10<0.5}\tau)$  within  $q_{0.10} < q_{0.10rat}/2$ , relative values of summarized exceedance  $\sum(q_{0.10rat}/2\tau)_{ex<0.5} / \sum(q_{0.10rat}/2\tau)$ , and summarized refrigeration energy consumed  $\sum(q_{0.10}\tau)_{<0.5} / \sum(q_{0.10rat}/2\tau)$ .

The following correlations are used:  $\sum(q_{0.10\text{rat}/2\tau})_{\text{ex}<0.5} = \sum(q_{0.10\text{rat}/2\tau} - q_{0.10<0.5\tau})_{\text{ex}<0.5}$ ;  $q_{0.10\text{rat}/2\text{ex}<0.5} = q_{0.10\text{rat}/2} - q_{0.10<0.5}$ ;  $\sum(q_{0.10\text{rat}/2\tau})_{\text{ex}<0.5} / \sum(q_{0.10\text{rat}/2\tau})$ ; and the criteria developed are:  $\text{LL} = \sum(q_{0.10\tau})_{<0.5} / \sum(q_{0.10\text{rat}/2\tau})$ ,  $\text{LL}_{\text{red}} = \sum(q_{0.10\text{rat}/2\tau})_{\text{ex}<0.5} / \sum(q_{0.10\text{rat}/2\tau})$ ,  $\text{LL} = 1 - \text{LL}_{\text{red}}$ .

Thus, the character of the summarized refrigeration energy exceedance curve  $\sum(q_{0.10\text{rat}/2\text{ex}\tau})_{<0.5}$  can serve as the indicator for its recoup to cover the peak loads and to reduce the installed refrigeration capacity as a result (Figures 3 and 4).

In addition, the relative summarized refrigeration energy exceedance  $\sum(q_{0.10\text{rat}/2\text{ex}\tau})_{<0.5} / \sum(q_{0.10\text{rat}/2\tau})$ , characterizing the level of loading in the unregulated load range, indirectly indicates the potential reduction in the LRL of the SRC.

The exceedance of the design refrigeration capacity  $q_{0.10\text{rat}}$  over the actual loads  $q_{0.10}$  is reflected in the booster refrigeration capacity  $q_{0.10-15}$  available for preconditioning outdoor air to 15 °C. Therefore, this is accepted as the object for the next step of the analysis aimed at partly stabilizing the heat load, leading to a reduction in the booster load range from  $q_{0.10-15}$  to  $q_{0.10-20}$  as the regulated load range and the LRL of the SRC by recouping the refrigeration energy exceedance.

In the approach to partly offset the current heat load fluctuations due to the reduction in the refrigeration capacity  $q_{0.15}$ , the value  $q_{0.20\text{rat}}$  required for conditioning air to 20 °C might be accepted as the artificial threshold temperature  $t_{\text{thr}} = 20$  °C and the range of heat loads  $q_{0.10-20}$  as an artificially (relatively) stable range in the initial approximation (Figure 5).

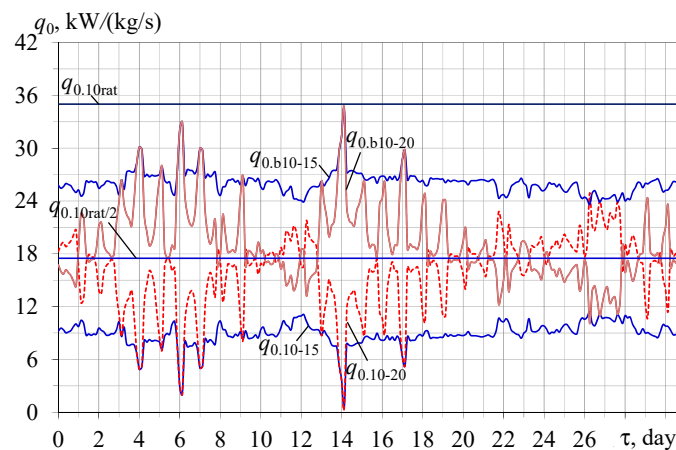


**Figure 5.** Actual values of refrigeration capacities  $q_{0.10-15,20}$  for further conditioning of air from 15 °C and 20 °C to 10 °C and residual booster values  $q_{0.10-15,20}$  for preconditioning ambient air to 15 °C and 20 °C:  $q_{0.10-15,20} = q_{0.10} - q_{0.15,20}$ ,  $q_{0.10-15,20} = q_{0.10\text{rat}} - q_{0.10-15,20}$ .

The extended artificially (relatively) stable heat load  $q_{0.10-20}$  might be considered an increased basic design value  $q_{0.10-20}$  compared to its initial value of  $q_{0.10-15}$ . Such an approach, as the initial step in the approximation (based on initial, not reduced, value  $q_{0.10\text{rat}}$  and  $\text{LRL} = 0.5$ ), is approved by the calculation results in Figure 6.

The following correlations are used:  $q_{0.10-15,20} = q_{0.10} - q_{0.15,20}$ ,  $q_{0.10-15,20} = q_{0.10\text{rat}} - q_{0.10-15,20}$ ; and the correlations for the developed criteria are:  $\text{LRL} = \sum(q_{0.10-15,20}\tau) / \sum(q_{0.10\text{rat}}\tau)$ ,  $1 - \text{LRL} = \sum(q_{0.10-15,20}\tau) / \sum(q_{0.10\text{rat}}\tau)$ .

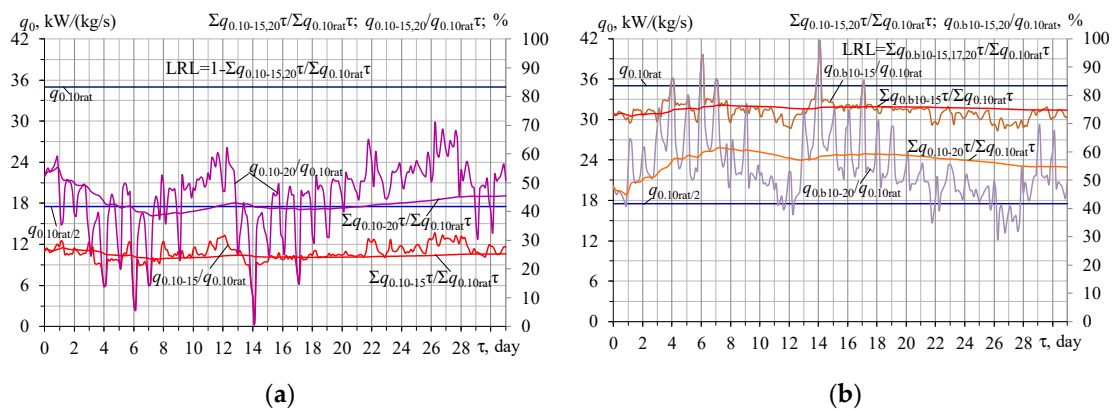


**Figure 6.** Relative values of refrigeration capacities  $q_{0.10-15,20}/q_{0.10rat}$  for further conditioning of air from 15 °C and 20 °C to 10 °C, and corresponding relative summarized refrigeration energy consumed  $\Sigma(q_{0.10-15,20}\tau)/\Sigma(q_{0.10rat}\tau)$  (a), relative residual booster refrigeration capacities  $q_{0.b10-15,20}/q_{0.10rat}$  and corresponding relative summarized booster refrigeration energy  $\Sigma(q_{0.b10-15,20}\tau)/\Sigma(q_{0.10rat}\tau)$  (b): (a)— $q_{0.10-15,20}$ ; (b)— $q_{0.b10-15,20}$ .

As previously established, at the same value of LRL (LRL = 0.5 in our example), the higher the value of the intermediate threshold temperature  $t_{thr}$ , id est, the larger the range of artificially unchangeable load,  $q_{0.10-20}$  compared to  $q_{0.10-15}$ , and the more efficient the performance of the SRC with an LRL of 50%; the value of  $q_{0.10-20}$  is closer to  $q_{0.10rat}/2$  compared to  $q_{0.10-15}$  at LRL = 0.5 (Figure 6a). This is also supported by the values of the relative summarized refrigeration energy consumed  $\Sigma(q_{0.10-20}\tau)/\Sigma(q_{0.10rat}\tau)$  and the corresponding available relative summarized booster refrigeration energy  $\Sigma(q_{0.b10-20}\tau)/\Sigma(q_{0.10rat}\tau)$  closer to  $q_{0.10rat}/2$  compared to  $\Sigma(q_{0.10-15}\tau)/\Sigma(q_{0.10rat}\tau)$  and  $\Sigma(q_{0.b10-15}\tau)/\Sigma(q_{0.10rat}\tau)$  (Figure 6).

As a result, due to the recouping of the refrigeration energy exceedance  $\Sigma(q_{0.10rat}/2_{ex}\tau) < 0.5$  (Figure 4), the fluctuations of the current subconditioning heat loads (refrigeration capacities)  $q_{0.10-20}/q_{0.10rat}$  and corresponding booster preconditioning heat loads (refrigeration capacities)  $q_{0.b10-20}/q_{0.10rat}$ , initially characterized by significant deviations (amplitudes), are narrowed by about 1.5 to 2.0 times according to the ratios  $q_{0.10-15}/q_{0.10-20}$  and  $q_{0.b10-15}/q_{0.b10-20}$ , respectively. They follow the trend of the relative summarized refrigeration energy consumed  $\Sigma(q_{0.10-20}\tau)/\Sigma(q_{0.10rat}\tau)$  and  $q_{0.b10-20}/q_{0.10rat}$ , but with considerably fewer deviations (amplitudes), similar to those for  $q_{0.10-15}/q_{0.10rat}$  and  $q_{0.b10-15}/q_{0.10rat}$  (Figure 6).

The results of the refrigeration energy exceedance recuperation for covering the booster preconditioning load  $q_{0.20}$  and  $q_{0.15}$  using the reduced rational refrigeration capacity  $q_{0.20rat}$  are presented in Figures 7 and 8.

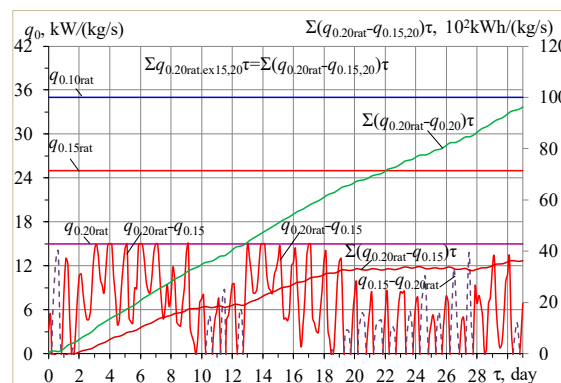


**Figure 7.** Actual values of rational refrigeration capacity  $q_{0.20rat}$  exceedance  $q_{0.20rat} - q_{0.15}$  above  $q_{0.15}$  and its deficit  $q_{0.15} - q_{0.20rat}$ , and summarized monthly refrigeration energy exceedance  $\Sigma(q_{0.20rat} - q_{0.20})\tau$  over  $q_{0.20}$  and  $\Sigma(q_{0.20rat} - q_{0.15})\tau$  over  $q_{0.15}$ .

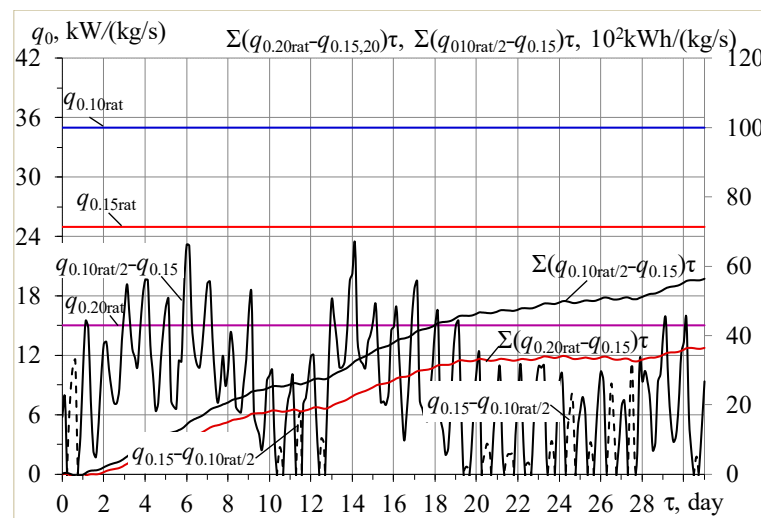


**Figure 8.** Actual values of rational refrigeration capacity  $q_{0.10rat/2}$  exceedance  $q_{0.10rat/2} - q_{0.15}$  above  $q_{0.15}$  and its deficit  $q_{0.15} - q_{0.10rat/2}$ , summarized monthly refrigeration energy  $\sum q_{0.10rat/2}\tau$  exceedance  $\sum(q_{0.10rat/2} - q_{0.15})\tau$  over  $q_{0.15}$ , and summarized refrigeration  $\sum q_{0.20rat}\tau$  exceedance  $\sum q_{0.20rat.ex15}\tau = \sum(q_{0.20rat} - q_{0.15})\tau$  over  $q_{0.15}$ .

The following correlations are used:  $q_{0.20rat.ex15} = q_{0.20rat} - q_{0.15}$ ,  $q_{0.20rat.def15} = q_{0.15} - q_{0.20rat}$ ,  $\sum q_{0.20rat.ex20}\tau = \sum(q_{0.20rat} - q_{0.20})\tau$ ,  $\sum q_{0.20rat.ex15}\tau = \sum(q_{0.20rat} - q_{0.15})\tau$ .

As Figure 7 shows, the rising character of the available summarized exceedance of the refrigeration energy curve  $\sum(q_{0.20rat} - q_{0.20})\tau$  indicates that a design refrigeration capacity of  $q_{0.20rat}$  is sufficient not only to offset its actual deficit  $q_{0.20} - q_{0.20rat}$ , but also to enable the deeper cooling of outdoor air to 15 °C from 20 °C by recouping the reserved refrigeration energy  $\sum(q_{0.20rat} - q_{0.15})\tau$  at lowered actual heat loads  $q_{0.15}$ .

As observed, the actual values of the available exceedance  $q_{0.20rat} - q_{0.15}$  of the rational refrigeration capacity  $q_{0.20rat}$  above  $q_{0.15}$  dominate their deficit (lack)  $q_{0.15} - q_{0.20rat}$ .

The practically constant values  $\sum(q_{0.20rat} - q_{0.15})\tau$  between 10 ... 13 and 20 ... 26 July demonstrate that the daily values of deficit  $\sum(q_{0.15} - q_{0.20rat})\tau$  are compensated by their values of reserved refrigeration energy  $\sum(q_{0.20rat} - q_{0.15})\tau$ . However, the short time-lowering values  $\sum(q_{0.20rat} - q_{0.15})\tau$  during 27 and 28 July reveal the presence of a small daily refrigeration capacity deficit of  $q_{0.20rat}$ .

In order to avoid a daily refrigeration capacity deficit of  $q_{0.20rat}$ , it is necessary to increase the design refrigeration capacity, for instance, to  $q_{0.10rat/2} = 17.5$  kW/(kg/s) instead of  $q_{0.20rat} = 15$  kW/(kg/s) (Figure 8).

The following correlations are used:  $q_{0.10rat/2.ex15} = q_{0.10rat/2} - q_{0.15}$ ,  $q_{0.10rat/2.def15} = q_{0.15} - q_{0.10rat/2}$ ,  $\sum q_{0.10rat/2.ex15}\tau = \sum(q_{0.10rat/2} - q_{0.15})\tau$ ,  $\sum q_{0.20rat.ex15}\tau = \sum(q_{0.20rat} - q_{0.15})\tau$ .

The continuously rising character of the available summarized exceedance of the refrigeration energy curve  $\sum(q_{0.10rat/2} - q_{0.15})\tau$  demonstrates that the increased refrigeration capacity  $q_{0.10rat/2}$  compared to  $q_{0.20rat}$  is able to cover its actual deficit  $q_{0.15} - q_{0.10rat/2}$  by the daily recouping of the reserved refrigeration energy  $\sum(q_{0.10rat/2} - q_{0.15})\tau$  at lowered current heat loads  $q_{0.10}$ , as well as with a significant monthly exceedance of 5600 kWh/(kg/s) (Figure 8).

Meanwhile, proceeding from the use of  $q_{0.20rat}$  as the design refrigeration capacity for conditioning outdoor air to 15 °C instead of  $q_{0.15rat}$  (Figure 7), the overall design refrigeration capacity for conditioning outdoor air to 10 °C can be reduced to  $q_{0.10red} = 25$  kW/(kg/s) against  $q_{0.10rat} = 35$  kW/(kg/s), that is, by the value of the difference  $q_{0.15rat} - q_{0.20rat} = 10$  kW/(kg/s) according to Figure 1. In reality, we can use  $q_{0.10red} = q_{0.15rat}$ . The results of the calculations are presented in Figure 9.

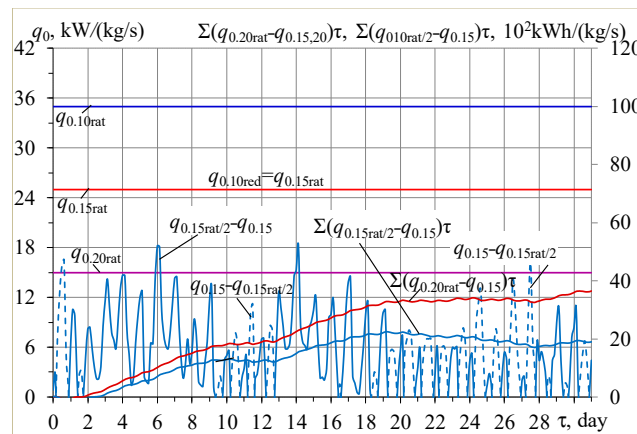


**Figure 9.** Reduced rational value  $q_{0.10red} = q_{0.15rat}$  for conditioning outdoor air to 10 °C using reserved refrigeration energy, actual refrigeration capacities  $q_{0.15}$  needed for conditioning outdoor air to 15 °C, reduced refrigeration capacity  $q_{0.15rat}/2$  exceedance  $q_{0.15rat}/2 - q_{0.15}$  above  $q_{0.15}$  and its deficit  $q_{0.15} - q_{0.15rat}/2$ , summarized monthly refrigeration energy exceedance  $\Sigma(q_{0.15rat}/2 - q_{0.15})\tau$  and  $\Sigma(q_{0.20rat} - q_{0.15})\tau$  over  $q_{0.15}$ .

The following correlations are used:  $q_{0.10red} = q_{0.15rat}$ ,  $q_{0.15rat}/2.ex15 = q_{0.15rat}/2 - q_{0.15}$ ,  $q_{0.15rat}/2.def15 = q_{0.15} - q_{0.15rat}/2$ ,  $\Sigma q_{0.15rat}/2.ex15\tau = \Sigma(q_{0.15rat}/2 - q_{0.15})\tau$ ,  $\Sigma q_{0.20rat}.ex15\tau = \Sigma(q_{0.20rat} - q_{0.15})\tau$ .

As Figure 9 shows, in the case of applying the value of the refrigeration capacity  $q_{0.10red} = q_{0.15rat}/2$  instead of  $q_{0.10rat}/2$ , id est,  $q_{0.15rat}$  instead of  $q_{0.10rat}$  as a design value, within nearly half of a month, the current values of deficit  $q_{0.15} - q_{0.15rat}/2$  are not covered by the actual values of the available exceedance  $q_{0.15rat}/2 - q_{0.15}$  of the rational refrigeration capacity  $q_{0.15rat}/2$  above  $q_{0.15}$ , leading to a reduction in the summarized curve  $\Sigma(q_{0.15rat}/2 - q_{0.15})\tau$ . However, the monthly exceedance of the refrigeration energy  $\Sigma(q_{0.15rat}/2 - q_{0.15})\tau = 2000 \text{ kWh}/(\text{kg/s})$  is much less than  $\Sigma(q_{0.20rat} - q_{0.15})\tau = 3500 \text{ kWh}/(\text{kg/s})$  (Figure 9).

The increase in the available summarized exceedance of the refrigeration energy curve  $\Sigma(q_{0.20rat} - q_{0.15})\tau$  indicates that a design refrigeration capacity of  $q_{0.20rat}$  is sufficient to cover its actual deficit  $q_{0.15} - q_{0.20rat}$ , even for deeper cooling of outdoor air to 15 °C instead of 20 °C by recouping the reserved refrigeration energy  $\Sigma(q_{0.20rat} - q_{0.15})\tau$  at lowered current heat loads  $q_{0.20}$ .

The generalized results on the values of the summarized monthly refrigeration energy exceedance  $\Sigma(q_{0.10rat}/2 - q_{0.15})\tau$ ,  $\Sigma(q_{0.20rat} - q_{0.15})\tau$ , and  $\Sigma(q_{0.15rat}/2 - q_{0.15})\tau$  over  $q_{0.15}$  are presented in Figure 10.

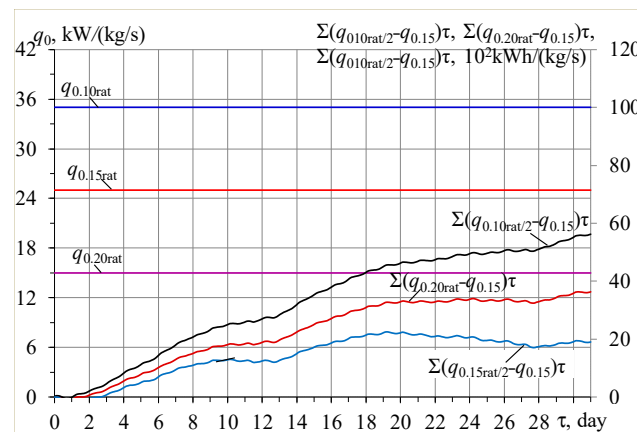


**Figure 10.** Rational values of refrigeration capacities  $q_{0.10rat}$ ,  $q_{0.15rat}$ , and  $q_{0.20rat}$  for conditioning outdoor air to 10 °C, 15 °C, and 20 °C, respectively, and summarized monthly refrigeration energy exceedance  $\Sigma(q_{0.10rat}/2 - q_{0.15})\tau$ ,  $\Sigma(q_{0.20rat} - q_{0.15})\tau$ , and  $\Sigma(q_{0.15rat}/2 - q_{0.15})\tau$  over  $q_{0.15}$ .

The following correlations are used:  $\sum q_{0.10rat}/2_{ex15}\tau = \sum(q_{0.10rat}/2 - q_{0.15})\tau$ ,  $\sum q_{0.20rat.ex15}\tau = \sum(q_{0.20rat} - q_{0.15})\tau$ ,  $\sum q_{0.15rat}/2_{ex15}\tau = \sum(q_{0.15rat}/2 - q_{0.15})\tau$ .

As Figure 10 shows, in the case of applying the value of the reduced refrigeration capacity  $q_{0.10}/2_{red} = q_{0.15rat}/2$  instead of  $q_{0.10rat}/2$ , id est,  $q_{0.15rat}$  instead of  $q_{0.10rat}$  as a design value, within nearly half of the month, the current values of deficit  $q_{0.15} - q_{0.15rat}/2$  are not covered by the actual values of the available exceedance  $q_{0.15rat}/2 - q_{0.15}$  of the rational refrigeration capacity  $q_{0.15rat}/2$  above  $q_{0.15}$ , and is accompanied by a reduction in the summarized curve  $\sum(q_{0.15rat}/2 - q_{0.15})\tau$ . However, with this, the monthly exceedance of the refrigeration energy is the lowest  $\sum(q_{0.15rat}/2 - q_{0.15})\tau = 2000 \text{ kWh}/(\text{kg/s})$  and the lowest value of the level of regulated loading is expected.

The application of the reduced refrigeration capacity  $q_{0.20rat}$  for conditioning air to  $15^\circ\text{C}$  instead of  $q_{0.15rat}$   $20^\circ\text{C}$  by recouping the reserved refrigeration energy  $\sum(q_{0.20rat} - q_{0.15})\tau$  generally covers the deficit, and is accompanied by the increase in the available summarized exceedance of the refrigeration energy curve  $\sum(q_{0.20rat} - q_{0.15})\tau$ , excluding two days (27 and 28 July). With this, the monthly exceedance of the refrigeration energy is  $\sum(q_{0.20rat} - q_{0.15})\tau = 3500 \text{ kWh}/(\text{kg/s})$  and a higher LRL value is expected.

The largest value of the monthly exceedance of refrigeration energy  $\sum(q_{0.10rat}/2 - q_{0.15})\tau = 5500 \text{ kWh}/(\text{kg/s})$  takes place without recouping the reserved refrigeration energy, providing a continuous increase in the summarized curve  $\sum(q_{0.10rat}/2 - q_{0.15})\tau$ .

The following correlations are used:  $q_{0.10red} = q_{0.15rat}$ ,  $\sum(q_{0.b10-15rat}\tau)/\sum(q_{0.15rat}\tau)$ ,  $\sum(q_{0.b10-20.rat15}\tau)/\sum(q_{0.15rat}\tau)$ ,  $q_{0.b10-15,20} = q_{0.10rat} - q_{0.10-15,20}$ ;  $q_{0.b10-15,20.rat15} = q_{0.15rat} - q_{0.10-15,20}$ ; and the correlations for the developed criteria are:  $LRL_{10-15,20} = \sum(q_{0.b10-15,20}\tau)/\sum(q_{0.10rat}\tau)$ ,  $LRL_{10-15,20red} = \sum(q_{0.b10-15,20.rat15}\tau)/\sum(q_{0.15rat}\tau)$ .

Figure 11 shows the values of the reduced relative summarized booster refrigeration energy  $\sum(q_{0.b10-15rat}\tau)/\sum(q_{0.15rat}\tau) \approx 0.65$  at reduced design refrigeration capacity  $q_{0.15red} = q_{0.15rat}$ , gained due to recuperation, against their values  $\sum(q_{0.b10-15}\tau)/\sum(q_{0.10rat}\tau) \approx 0.75$  at  $q_{0.10rat}$  without recuperation for  $t_{thr} = 15^\circ\text{C}$  and  $\sum(q_{0.b10-20.rat15}\tau)/\sum(q_{0.15rat}\tau) \approx 0.4$  against  $\sum(q_{0.b10-20rat}\tau)/\sum(q_{0.10rat}\tau) \approx 0.55$  at  $q_{0.10rat}$  without recuperation for the artificial air threshold temperature  $t_{thr} = 20^\circ\text{C}$ . Thus, due to reserved refrigeration energy recuperation, the design refrigeration capacity is reduced to  $q_{0.10red} = q_{0.15rat} = 25 \text{ kW}/(\text{kg/s})$  against the initial value of  $q_{0.10rat} = 35 \text{ kW}/(\text{kg/s})$ , id est, by about 30%.

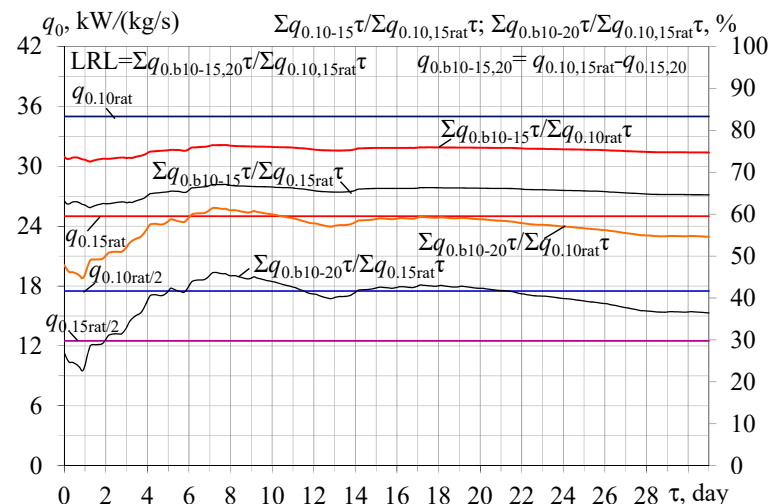


**Figure 11.** Values of relative summarized booster refrigeration energy  $\sum(q_{0.b10-15}\tau)/\sum(q_{0.10rat}\tau)$  and  $\sum(q_{0.b10-20}\tau)/\sum(q_{0.10rat}\tau)$  available for conditioning air to  $15^\circ\text{C}$  and  $20^\circ\text{C}$ , reduced summarized refrigeration energy  $\sum(q_{0.b10-15rat}\tau)/\sum(q_{0.15rat}\tau)$  and  $\sum(q_{0.b10-20.rat15}\tau)/\sum(q_{0.15rat}\tau)$ , generated according to reduced value of design refrigeration capacity  $q_{0.15red} = q_{0.15rat}$ .

Furthermore, according to the rising air threshold temperature from the initial value of  $t_{thr} = 15^\circ\text{C}$  at  $q_{0.10rat}$  without recuperation to the artificial increased value of  $t_{thr} = 20^\circ\text{C}$

°C at reduced design refrigeration capacity  $q_{0.10red} = q_{0.15rat}$  with recuperation, the LRL value for the SRC reduces from an initial  $LRL_{10-15} = \sum(q_{0.b10-15}\tau)/\sum(q_{0.10rat}\tau)$  of about 0.75 to  $LRL_{10-20red} = \sum(q_{0.b10-20.rat15}\tau)/\sum(q_{0.15rat}\tau)$  of about 0.4.

This conclusion is also supported by the results of the calculation of the current  $LRL_{10-15,20red.cur}$  as current relative values of reduced residual booster refrigeration capacities  $LRL_{10-15red.cur} = q_{0.b10-15rat}/q_{0.15rat}$  and  $LRL_{10-20red.cur} = q_{0.b10-20.rat15}/q_{0.15rat}$  available for conditioning air to 10 °C at  $t_{thr} = 15$  °C and 20 °C, referring to the reduced design refrigeration capacity  $q_{0.15rat}$  and the corresponding summarized  $LRL_{10-15,20red}$  as reduced summarized refrigeration energy  $LRL_{10-15red} = \sum(q_{0.b10-15rat}\tau)/\sum(q_{0.15rat}\tau)$  and  $\sum(q_{0.b10-20.rat15}\tau)/\sum(q_{0.15rat}\tau)$ , generated according to the reduced value of the design refrigeration capacity  $q_{0.15rat}$  (Figure 12).

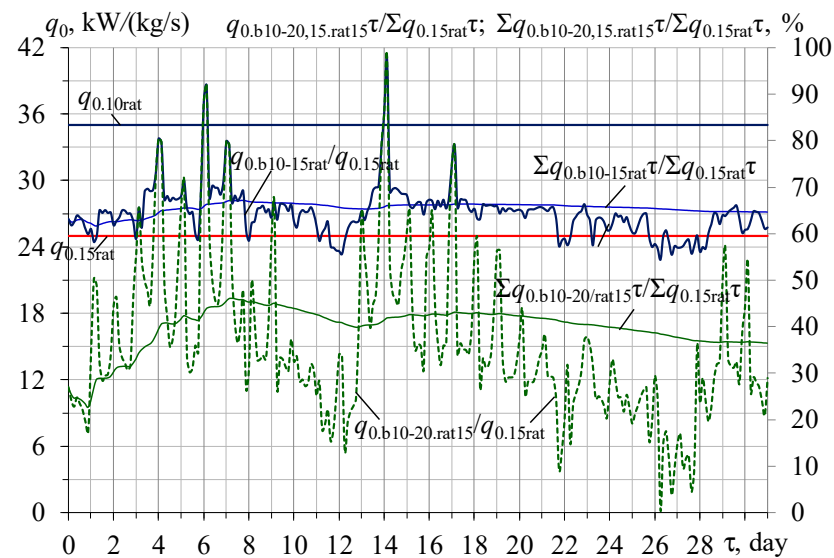


**Figure 12.** Actual relative reduced booster refrigeration capacities  $q_{0.b10-15rat}/q_{0.15rat}$  and  $q_{0.b10-20.rat15}/q_{0.15rat}$  available for conditioning air to 10 °C at threshold temperatures of  $t_{thr} = 15$  °C and 20 °C and corresponding reduced summarized refrigeration energy  $\sum(q_{0.b10-15rat}\tau)/\sum(q_{0.15rat}\tau)$  and  $\sum(q_{0.b10-20.rat15}\tau)/\sum(q_{0.15rat}\tau)$ , generated according to reduced design refrigeration capacity  $q_{0.10red} = q_{0.15rat}$ .

The following correlations are used:  $q_{0.10red} = q_{0.15rat}$ ,  $q_{0.b10-15rat}/q_{0.15rat}$ ,  $q_{0.b10-20.rat15}/q_{0.15rat}$ ,  $q_{0.b10-15rat} = q_{0.15rat} - q_{0.10-15}$ ,  $q_{0.b10-20.rat15} = q_{0.15rat} - q_{0.10-20}$ ,  $\sum(q_{0.b10-15rat}\tau)/\sum(q_{0.15rat}\tau)$ ,  $\sum(q_{0.b10-20.rat15}\tau)/\sum(q_{0.15rat}\tau)$ ; and the correlations for the developed criteria are:  $LRL_{10-15red} = \sum(q_{0.b10-15rat}\tau)/\sum(q_{0.15rat}\tau)$ ;  $LRL_{10-20red} = \sum(q_{0.b10-20.rat15}\tau)/\sum(q_{0.15rat}\tau)$ ;  $LRL_{10-15red.cur} = q_{0.b10-15rat}/q_{0.15rat}$ ;  $LRL_{10-20red.cur} = q_{0.b10-20.rat15}/q_{0.15rat}$ .

As Figure 12 shows, the values of the summarized  $LRL_{10-15,20red}$ , affected by the current  $LRL_{10-15,20red.cur}$ , strictly follow the latter, justifying all of the methodological innovative approaches and revealing the technical solutions, resulting in the enhancement of the obtained output.

Thus, an advanced reserved refrigeration energy recuperation approach to reduce the design refrigeration capacity for a VRF-type ACS and the level of regulated load, id est, SRC operation efficiency, has been developed.

#### 4. Conclusions

An advanced methodology of designing VRF systems with SRCs has been developed to distribute heat flows proceeding from the peculiarities of the different characteristics of heat loads while processing outdoor air, involving changeable loads for the preconditioning of outdoor air to a definite threshold temperature and practically unchangeable loads for further conditioning of the air to a set temperature value.

The methodology makes it possible to reveal the reserves for the enhancement of the SRCs and the operational efficiency of the whole VRF system by recouping the refrigeration energy, reserved at lowered heat loads, to match the current refrigeration consumption at reduced refrigeration capacities.

The methodology helps to determine the values of reduced design refrigeration capacities to provide a continuously increasing growth of the monthly summarized refrigeration energy, reserved at reduced loading.

The recuperation of the reserved refrigeration energy helps to reduce the design refrigeration capacity of the VRF system using SRCs by about 20% for temperate climatic conditions.

Furthermore, under increasing air temperature conditions, limiting the range of the regulated fluctuated loads and narrowing this range through reserved refrigeration recuperation reduces the LRL value of the SRC by almost half.

All of the methodological innovative approaches aimed to enhance the obtained output are justified by the calculations of the current refrigeration capacities and the summarized refrigeration energy characterized the operation efficiency of the VRF systems with SRCs.

It should be noted that all quantitative results were obtained for the specific climatic conditions of the object with minimal assumptions and limitations. Methodological innovative approaches, which are implemented in this work through phenomenological modeling, can be extended and applied to any particular case.

Thus, an advanced approach to reserved refrigeration energy recuperation to reduce the design refrigeration capacity of VRF-type ACSs and the required level of the regulated load, *id est*, SRC operation efficiency, has been developed.

Further investigations are required to reveal the methodological peculiarities of ACS design to determine the rational refrigeration capacities to avoid oversizing in different climates (European temperate, Mediterranean, Middle East, subtropical, tropical, and other climatic regions) as well as for railway ACSs and engine-intake air cooling including driving engines in trigeneration and marine power plants.

**Author Contributions:** Conceptualization, M.R. (30%), A.R. (25%), E.T. (15%), H.K. (10%), and R.R. (20%); methodology, M.R. (30%), A.R. (25%), E.T. (15%), H.K. (10%), and R.R. (20%); software, M.R. (25%), A.R. (30%), E.T. (10%), H.K. (10%), and R.R. (25%); validation, M.R. (25%), A.R. (30%), E.T. (10%), H.K. (15%), and R.R. (20%); formal analysis, M.R. (30%), A.R. (25%), E.T. (10%), H.K. (15%), and R.R. (20%); writing—original draft preparation, M.R. (30%), A.R. (25%), E.T. (10%), H.K. (15%), and R.R. (20%); writing—review and editing, M.R. (30%), A.R. (25%), E.T. (15%), H.K. (10%), and R.R. (20%). All authors have read and agreed to the published version of the manuscript.

**Funding:** The project is supported by the program of the Minister of Science and Higher Education under the name: “Regional Initiative of Excellence” in 2019–2023 project number 025/RID/2018/19 financing amount PLN 12,000,000.

**Data Availability Statement:** Not applicable.

**Conflicts of Interest:** The authors declare no conflict of interest.

## Nomenclature and Units

ACS	air conditioning system
LL	level of load
LRL	level of regulated load
SRC	speed-regulated compressor
VRF	variable refrigerant flow

## Symbols and units

$b$	booster	
$c_a$	specific heat of humid air	kJ/(kg·K)
$d_{amb}$	absolute humidity	g/kg
$G_a$	air mass flow rate	kg/s
$Q_0$	total refrigeration capacity	kW
$q_0$	specific refrigeration capacity (per unit air mass flow rate)	kW/(kg/s)
$q_0\tau$	specific refrigeration energy (per unit air mass flow rate)	kW/(kg/s)
$t_{amb}$	ambient (outdoor) air temperature	K, °C
$t_{a2}$	target air temperature	K, °C
$\xi$	specific heat ratio of the total heat (latent and sensible) removed from air to sensible heat	
$\tau$	time interval	h
$\varphi_{amb}$	relative humidity	%
$\Delta t$	temperature decrease	K, °C
$\Sigma(q_0\tau)$	annual (monthly) specific refrigeration energy consumption (per unit air mass rate)	kWh/(kg/s)
Subscripts		
10, 15, 20	air temperature	K, °C
a	air	
amb	ambient	
b	booster	
max	maximum	
rat	rational	

## References

- Gayeski, N.T.; Armstrong, P.R.; Norford, L.K. Predictive pre-cooling of thermo-active building systems with low-lift chillers. *HVAC&R Res.* **2012**, *18*, 1–16.
- Southard, L.E.; Liu, X.; Spittler, J.D. Performance of HVAC systems at ASHRAE HQ. *ASHRAE J.* **2014**, *56*, 14–24.
- Khliyeva, O.; Shestopalov, K.; Ierin, V.; Zhelezny, V.; Chen, G.; Gao, N. Environmental and energy comparative analysis of expediency of heat-driven and electrically-driven refrigerators for air conditioning application. *Appl. Therm. Eng.* **2022**, *219*, 119533. [\[CrossRef\]](#)
- Gluesenkamp, K.; Hwang, Y.; Radermacher, R. High efficiency micro trigeneration systems. *Appl. Therm. Eng.* **2013**, *50*, 6. [\[CrossRef\]](#)
- Yang, Z.; Korobko, V.; Radchenko, M.; Radchenko, R. Improving thermoacoustic low temperature heat recovery systems. *Sustainability* **2022**, *14*, 12306. [\[CrossRef\]](#)
- Yang, Z.; Radchenko, R.; Radchenko, M.; Radchenko, A.; Kornienko, V. Cooling potential of ship engine intake air cooling and its realization on the route line. *Sustainability* **2022**, *14*, 1974710. [\[CrossRef\]](#)
- Mohapatra, A.K. Comparative analysis of inlet air cooling techniques integrated to cooled gas turbine plant. *J. Energy Inst.* **2015**, *88*, 344–358. [\[CrossRef\]](#)
- Radchenko, A.; Radchenko, N.; Tsoy, A.; Portnoi, B.; Kantor, S. Increasing the efficiency of gas turbine inlet air cooling in actual climatic conditions of Kazakhstan and Ukraine. In *AIP Conference Proceedings 2020*; AIP Publishing LLC: Melville, NY, USA, 2020. [\[CrossRef\]](#)
- Radchenko, A.; Radchenko, M.; Mikielwicz, D.; Pavlenko, A.; Radchenko, R.; Forduy, S. Energy saving in trigeneration plant for food industries. *Energies* **2022**, *15*, 1163. [\[CrossRef\]](#)
- Rocha, M.S.; Andreos, R.; Simões-Moreira, J.R. Performance tests of two small trigeneration pilot plants. *Appl. Therm. Eng.* **2012**, *41*, 84–91. [\[CrossRef\]](#)
- Yu, Z.; Shevchenko, S.; Radchenko, M.; Shevchenko, O.; Radchenko, A. Methodology of Designing Sealing Systems for Highly Loaded Rotary Machines. *Sustainability* **2022**, *14*, 15828. [\[CrossRef\]](#)
- Khliyeva, O. New indicator for life cycle greenhouse gases emission assessment of household refrigerating appliances. *Environ. Probl.* **2019**, *4*, 39–44. [\[CrossRef\]](#)
- Radchenko, A.; Scurtu, I.-C.; Radchenko, M.; Forduy, S.; Zubarev, A. Monitoring the efficiency of cooling air at the inlet of gas engine in integrated energy system. *Therm. Sci.* **2022**, *26*, 185–194. [\[CrossRef\]](#)
- Radchenko, A.; Radchenko, M.; Koshlak, H.; Radchenko, R.; Forduy, S. Enhancing the efficiency of integrated energy system by redistribution of heat based of monitoring data. *Energies* **2022**, *15*, 8774. [\[CrossRef\]](#)
- Radchenko, M.; Mikielwicz, D.; Andreev, A.; Vanyeyev, S.; Savenkov, O. Efficient ship engine cyclic air cooling by turboexpander chiller for tropical climatic conditions. In *Integrated Computer Technologies in Mechanical Engineering—2020*; Nechyporuk, M., Pavlikov, V., Kritskiy, D., Eds.; Lecture Notes in Networks and Systems; Springer: Cham, Switzerland, 2021; Volume 188, pp. 498–507.

16. Kornienko, V.; Radchenko, R.; Radchenko, M.; Radchenko, A.; Pavlenko, A.; Konovalov, D. Cooling cyclic air of marine engine with water-fuel emulsion combustion by exhaust heat recovery chiller. *Energies* **2022**, *15*, 248. [[CrossRef](#)]
17. Ghatos, S.; Taha-Janan, M.; Mehdari, A. Thermodynamic model of a single stage H<sub>2</sub>O-LiBr absorption cooling. In *E3S Web of Conferences 2021*; EDP Sciences: Les Ulis, France, 2021; Volume 234, p. 00091.
18. Radchenko, R.; Radchenko, N.; Tsoy, A.; Forduy, S.; Zybarev, A.; Kalinichenko, I. Utilizing the heat of gas module by an absorption lithium-bromide chiller with an ejector booster stage. In *AIP Conference Proceedings*; AIP Publishing LLC: Melville, NY, USA, 2020; Volume 2285, p. 030084. [[CrossRef](#)]
19. Yang, Z.; Kornienko, V.; Radchenko, M.; Radchenko, A.; Radchenko, R.; Pavlenko, A. Capture of pollutants from exhaust gases by low-temperature heating surfaces. *Energies* **2022**, *15*, 120. [[CrossRef](#)]
20. Yang, Z.; Kornienko, V.; Radchenko, M.; Radchenko, A.; Radchenko, R. Research of Exhaust Gas Boiler Heat Exchange Surfaces with Reduced Corrosion when Water-fuel Emulsion Combustion. *Sustainability* **2022**, *14*, 11927. [[CrossRef](#)]
21. Yang, Z.; Radchenko, M.; Radchenko, A.; Mikielewicz, D.; Radchenko, R. Gas turbine intake air hybrid cooling systems and a new approach to their rational designing. *Energies* **2022**, *15*, 1474. [[CrossRef](#)]
22. Radchenko, M.; Radchenko, A.; Radchenko, R.; Kantor, S.; Konovalov, D.; Kornienko, V. Rational loads of turbine inlet air absorption-ejector cooling systems. *Proc. Inst. Mech. Eng. Part A J. Power Energy* **2021**, *236*, 450–462. [[CrossRef](#)]
23. Tarasova, V.; Kuznetsov, M.; Kharlampidi, D.; Kostikov, A. Development of a vacuum-evaporative thermotransformer for the cooling system at a nuclear power plant. *East. -Eur. J. Enterp. Technol.* **2019**, *4*, 45–56. [[CrossRef](#)]
24. Radchenko, N. A concept of the design and operation of heat exchangers with change of phase. *Arch. Thermodyn.* **2004**, *25*, 3–19.
25. Mikielewicz, D.; Klugmann, M.; Wajs, J. Flow boiling intensification in minichannels by means of mechanical flow turbulising inserts. *Int. J. Therm. Sci.* **2013**, *65*, 79–91. [[CrossRef](#)]
26. Khliyeva, O.; Zhelezny, V.; Lukianov, T.; Lukianov, N.; Semenyuk, V.; Moreir, A.L.N.; Murshed, S.M.S.; Palomo del Barrio, E.; Nikulin, N. A new approach for predicting the pool boiling heat transfer coefficient of refrigerant R141b and its mixtures with surfactant and nanoparticles using experimental data. *J. Therm. Anal. Calorim.* **2020**, *142*, 2327–2339. [[CrossRef](#)]
27. Kruzal, M.; Bohdal, T.; Dutkowski, K.; Kuczyński, W.; Chliszcz, K. Current Research Trends in the Process of Condensation of Cooling Zeotropic Mixtures in Compact Condensers. *Energies* **2022**, *15*, 2241. [[CrossRef](#)]
28. Kuczyński, W.; Kruzal, M.; Chliszcz, K. A Regressive Model for Periodic Dynamic Instabilities during Condensation of R1234yf and R1234ze Refrigerants. *Energies* **2022**, *15*, 2117. [[CrossRef](#)]
29. Kruzal, M.; Bohdal, T.; Dutkowski, K.; Radchenko, M. The Effect of Microencapsulated PCM Slurry Coolant on the Efficiency of a Shell and Tube Heat Exchanger. *Energies* **2022**, *15*, 5142. [[CrossRef](#)]
30. Wajs, J.; Mikielewicz, D.; Jakubowska, B. Performance of the domestic micro ORC equipped with the shell-and-tube condenser with minichannels. *Energy* **2018**, *157*, 853–861. [[CrossRef](#)]
31. Kuczyński, W.; Kruzal, M.; Chliszcz, K. Regression Model of Dynamic Pulse Instabilities during Condensation of Zeotropic and Azeotropic Refrigerant Mixtures R404A, R448A and R507A in Minichannels. *Energies* **2022**, *15*, 1789. [[CrossRef](#)]
32. Pavlenko, A.M.; Koshlak, H. Application of thermal and cavitation effects for heat and mass transfer process intensification in multicomponent liquid media. *Energies* **2021**, *14*, 7996. [[CrossRef](#)]
33. Dąbrowski, P.; Klugmann, M.; Mikielewicz, D. Channel Blockage and Flow Maldistribution during Unsteady Flow in a Model Microchannel Plate heat Exchanger. *J. Appl. Fluid Mech.* **2019**, *12*, 1023–1035. [[CrossRef](#)]
34. Dąbrowski, P.; Klugmann, M.; Mikielewicz, D. Selected studies of flow maldistribution in a minichannel plate heat exchanger. *Arch. Thermodyn.* **2017**, *38*, 135–148. [[CrossRef](#)]
35. Kumar, R.; Singh, G.; Mikielewicz, D. A New Approach for the Mitigating of Flow Maldistribution in Parallel Microchannel Heat Sink. *J. Heat Transf.* **2018**, *140*, 72401–72410. [[CrossRef](#)]
36. Kumar, R.; Singh, G.; Mikielewicz, D. Numerical Study on Mitigation of Flow Maldistribution in Parallel Microchannel Heat Sink: Channels Variable Width Versus Variable Height Approach. *J. Electron. Packag.* **2019**, *141*, 21009–21011. [[CrossRef](#)]
37. Qian, Z.; Wang, Q.; Cheng, J.; Deng, J. Simulation investigation on inlet velocity profile and configuration parameters of louver fin. *Appl. Therm. Eng.* **2018**, *138*, 173–182. [[CrossRef](#)]
38. Yaïci, W.; Ghorab, M.; Entchev, E. 3D CFD study of the effect of inlet air flow maldistribution on plate-fin-tube heat exchanger design and thermal-hydraulic performance. *Int. J. Heat Mass Transf.* **2016**, *101*, 527–541. [[CrossRef](#)]
39. Zhelezny, V.; Khliyeva, O.; Lukianov, M.; Motovoy, I.; Ivchenko, D.A.; Faik, A.; Grosu, Y.; Nikulin, A.; Moreira, A.L.N. Thermodynamic properties of isobutane/mineral compressor oil and isobutane/mineral compressor oil/fullerenes C60 solutions. *Int. J. Refrig.* **2019**, *106*, 153–162. [[CrossRef](#)]
40. Dutkowski, K.; Kruzal, M. Microencapsulated PCM slurries' dynamic viscosity experimental investigation and temperature dependent prediction model. *Int. J. Heat Mass Transf.* **2019**, *145*, 118741. [[CrossRef](#)]
41. Chen, G.; Zhelezny, V.; Khliyeva, O.; Shestopalov, K.; Ierin, V. Ecological and energy efficiency analysis of ejector and vapor compression air conditioners. *Int. J. Refrig.* **2017**, *74*, 127–135. [[CrossRef](#)]
42. Yu, Z.; Løvås, T.; Konovalov, D.; Trushliakov, E.; Radchenko, M.; Kobalava, H.; Radchenko, R.; Radchenko, A. Investigation of thermopressor with incomplete evaporation for gas turbine intercooling systems. *Energies* **2023**, *16*, 20. [[CrossRef](#)]
43. Yang, Z.; Konovalov, D.; Radchenko, M.; Radchenko, R.; Kobalava, H.; Radchenko, A.; Kornienko, V. Analyzing the efficiency of thermopressor application for combustion engine cyclic air cooling. *Energies* **2022**, *15*, 2250. [[CrossRef](#)]

44. Konovalov, D.; Radchenko, M.; Kobalava, H.; Radchenko, A.; Radchenko, R.; Kornienko, V.; Maksymov, V. Research of characteristics of the flow part of an aerothermopressor for gas turbine intercooling air. *Proc. Inst. Mech. Eng. Part A J. Power Energy* **2021**, *236*, 634–646. [CrossRef]
45. Ierin, V.; Chen, G.; Volovyk, O.; Shestopalov, K. Hybrid two—Stage CO<sub>2</sub> transcritical mechanical compression—Ejector cooling cycle: Thermodynamic analysis and optimization. *Int. J. Refrig.* **2021**, *132*, 45–55. [CrossRef]
46. Chen, G.; Ierin, V.; Volovyk, O.; Shestopalov, K. An improved cascade mechanical compression—Ejector cooling cycle. *Energy* **2019**, *170*, 459–470. [CrossRef]
47. Fan, C.; Pei, D.; Wei, H. A novel cascade energy utilization to improve efficiency of double reheat cycle. *Energy Convers. Manag.* **2018**, *171*, 1388–1396. [CrossRef]
48. Shukla, A.K.; Singh, O. Thermodynamic investigation of parameters affecting the execution of steam injected cooled gas turbine based combined cycle power plant with vapor absorption inlet air cooling. *Appl. Therm. Eng.* **2017**, *122*, 380–388. [CrossRef]
49. Radchenko, M.; Radchenko, A.; Mikielwicz, D.; Radchenko, R.; Andreev, A. A novel degree-hour method for rational design loading. *Proc. Inst. Mech. Eng. Part A J. Power Energy* **2022**. [CrossRef]
50. Dhaka, S.; Mathur, J.; Garg, V. Combined effect of energy efficiency measures and thermal adaptation on air conditioned building in warm climatic conditions of India. *Energy Build.* **2012**, *55*, 351–360. [CrossRef]
51. Fumo, N.; Mago, P.J.; Smith, A.D. Analysis of combined cooling, heating, and power systems operating following the electric load and following the thermal load strategies with no electricity export. *Proc. Inst. Mech. Eng. Part A J. Power Energy* **2011**, *225*, 1016–1025. [CrossRef]
52. Cardona, E.; Piacentino, A. A methodology for sizing a trigeneration plant in mediterranean areas. *Appl. Therm. Eng.* **2003**, *23*, 15. [CrossRef]
53. Ortiga, J.; Bruno, J.C.; Coronas, A. Operational optimization of a complex trigeneration system connected to a district heating and cooling network. *Appl. Therm. Eng.* **2013**, *50*, 1536–1542. [CrossRef]
54. Suamir, I.N.; Tassou, S.A. Performance evaluation of integrated trigeneration and CO<sub>2</sub> refrigeration systems. *Appl. Therm. Eng.* **2013**, *50*, 1487–1495. [CrossRef]
55. Freschi, F.; Giaccone, L.; Lazzeroni, P.; Repetto, M. Economic and environmental analysis of a trigeneration system for food-industry: A case study. *Appl. Energy* **2013**, *107*, 157–172. [CrossRef]
56. Kavvadias, K.C.; Tosios, A.P.; Maroulis, Z.B. Design of a combined heating, cooling and power system: Sizing, operation strategy selection and parametric analysis. *Energy Convers. Manag.* **2010**, *51*, 833–845. [CrossRef]
57. Forsyth, J.L. Gas turbine inlet air chilling for LNG. *IGT Int. Liq. Nat. Gas Conf. Proc.* **2013**, *3*, 1763–1778.
58. Kalhori, S.B.; Rabiei, H.; Mansoori, Z. Mashhad trigeneration potential—An opportunity for CO<sub>2</sub> abatement in Iran. *Energy Conv. Manag.* **2012**, *60*, 106–114. [CrossRef]
59. Shubenko, A.; Babak, M.; Senetskyi, O.; Tarasova, V.; Goloshchapov, V.; Senetska, D. Economic assessment of the modernization perspectives of a steam turbine power unit to the ultra-supercritical operation conditions. *Int. J. Energy Res.* **2022**, *46*, 23530–23537. [CrossRef]
60. Popli, S.; Rodgers, P.; Eveloy, V. Trigeneration scheme for energy efficiency enhancement in a natural gas processing plant through turbine exhaust gas waste heat utilization. *Appl. Energy* **2012**, *93*, 623–636. [CrossRef]
61. Bai, Z.; Liu, Q.; Gong, L.; Lei, J. Application of a mid-/low-temperature solar thermochemical technology in the distributed energy system with cooling, heating and power production. *Appl. Energy* **2019**, *253*, 113491. [CrossRef]
62. Shukla, A.K.; Sharma, A.; Sharma, M.; Mishra, S. Performance improvement of simple gas turbine cycle with vapor compression inlet air cooling. *Mater. Today Proc.* **2018**, *5*, 19172–19180. [CrossRef]
63. Lee, Y.; Kim, W. Development of an Optimal Start Control Strategy for a Variable Refrigerant Flow (VRF). *Syst. Energ.* **2021**, *14*, 271. [CrossRef]
64. Radchenko, N.; Radchenko, A.; Tsoy, A.; Mikielwicz, D.; Kantor, S.; Tkachenko, V. Improving the efficiency of railway conditioners in actual climatic conditions of operation. In *AIP Conference Proceedings 2020*; AIP Publishing LLC: Melville, NY, USA, 2020; Volume 2285, p. 030072. [CrossRef]
65. Radchenko, N.; Trushliakov, E.; Radchenko, A.; Tsoy, A.; Shchesiuk, O. Methods to determine a design cooling capacity of ambient air conditioning systems in climatic conditions of Ukraine and Kazakhstan. In *AIP Conference Proceedings 2020*; AIP Publishing LLC: Melville, NY, USA, 2020; Volume 2285, p. 030074. [CrossRef]
66. Liu, C.; Zhao, T.; Zhang, J. Operational electricity consumption analyze of VRF air conditioning system and air conditioning system based on building energy monitoring and management system. *Procedia Eng.* **2015**, *121*, 1856–1863. [CrossRef]
67. Khatri, R.; Joshi, A. Energy performance comparison of inverter based variable refrigerant flow unitary AC with constant volume unitary AC. *Energy Procedia* **2017**, *109*, 18–26. [CrossRef]
68. Park, D.Y.; Yun, G.; Kim, K.S. Experimental evaluation and simulation of a variable refrigerant-flow (VRF) air-conditioning system with outdoor air processing unit. *Energy Build* **2017**, *146*, 122–140. [CrossRef]
69. Thornton, B.; Wagner, A. Variable Refrigerant Flow Systems. Seattle WA: Pacific Northwest National Laboratory. 2012. Available online: [http://www.gsa.gov/portal/mediaId/197399/fileName/GPG\\_Variable\\_Refrigerant\\_Flow\\_12-2012.action](http://www.gsa.gov/portal/mediaId/197399/fileName/GPG_Variable_Refrigerant_Flow_12-2012.action) (accessed on 19 January 2020).
70. Chen, J.; Xie, W. Analysis on load-undertaking of fan coil unit with fresh air system. *Adv. Mater. Res.* **2013**, *614*, 678–681. [CrossRef]

71. Zhu, Y.; Jin, X.; Du, Z.; Fang, X.; Fan, B. Control and energy simulation of variable refrigerant flow air conditioning system combined with outdoor air processing unit. *Appl. Therm. Eng.* **2014**, *64*, 385–395. [[CrossRef](#)]
72. Lee, J.H.; Yoon, H.J.; Im, P.; Song, Y.H. Verification of energy reduction effect through control optimization of supply air temperature in VRF-OAP system. *Energies* **2018**, *11*, 49. [[CrossRef](#)]
73. Pavlenko, A. Energy conversion in heat and mass transfer processes in boiling emulsions. *Therm. Sci. Eng. Prog.* **2020**, *15*, 00439. [[CrossRef](#)]
74. Pavlenko, A. Change of emulsion structure during heating and boiling. *Int. J. Energy A Clean Environ.* **2019**, *20*, 291–302. [[CrossRef](#)]
75. Radchenko, M.; Radchenko, A.; Trushliakov, E.; Pavlenko, A.M.; Radchenko, R. Advanced method of variable refrigerant flow (VRF) systems designing to forecast on site operation. Part 1: General approaches and criteria. *Energies* **2023**, *16*, 1381. [[CrossRef](#)]

**Disclaimer/Publisher’s Note:** The statements, opinions and data contained in all publications are solely those of the individual author(s) and contributor(s) and not of MDPI and/or the editor(s). MDPI and/or the editor(s) disclaim responsibility for any injury to people or property resulting from any ideas, methods, instructions or products referred to in the content.